Design requirements for aEVCS: Experimental analysis of inlet motion under load

Lars Knipschild*, Frederik Sicking, Bernd Künne, Marcel Bartz

Engineering Design and Product Development, TU Dortmund University, Dortmund, Germany

June 3, 2025

Abstract

This study investigates the dynamic behavior of electric vehicle (EV) inlets under various real-world load scenarios to contribute to the design requirements of automated EV charging systems (aEVCS). Inlet movements were tracked using a camera system in combination with AprilTag markers during typical usage scenarios such as passenger boarding and alighting, as well as cargo loading and unloading. The results show that while translational displacements generally remain within the limits defined by ISO 5474-5, rotational movements, especially in smaller vehicles, often exceed these thresholds. The findings underscore the impact of vehicle type and inlet location on displacement behavior, suggesting that current standards require refinement to better reflect real-world variability.

1 Introduction

The growing popularity of electric vehicles (EVs) requires efficient and user-friendly charging solutions to meet rising consumer expectations and support large-scale adoption [1]. Automatic electric vehicle charging systems (aEVCS) enhance convenience and safety, particularly benefiting individuals with physical disabilities [2]. Moreover, aEVCS play a critical role in supporting (partially) autonomous vehicles, where minimal human intervention requires fully automated infrastructure to ensure continuous and reliable operation [3].

However, the reliability of aEVCS depends on robust inlet detection and sufficient positioning accuracy to enable secure docking under real-world conditions [4]. In charging situations, the use of the vehicle should be as unrestricted as possible. Therefore, vehicle and thus inlet movements may occur. While ISO 5474-5 defines acceptable limits for inlet movement, it does not address the dynamic behavior of vehicles under real-world operating conditions [5]. This highlights the need for further research to understand how different load cases (LCs) affect inlet movement, which must be accounted for and compensated by the aEVCS. The aim is to establish relevant design requirements for interoperable aEVCS.

*Corresponding author: lars.knipschild@tu-dortmund.de

2 Method

This study investigates how different LCs affect the dynamic movement of the vehicle inlet in parked electric vehicles (EVs) across different vehicle types. The movement is tracked using a system that includes a monocular camera and a 3D-printed adapter mounted on the inlet, equipped with an attached AprilTag. The LCs simulate realistic scenarios that may occur during charging with an aEVCS.

Table 1 provides an overview of the LCs used for vehicle testing. The experiments are conducted on parked EVs. LC1 to LC4 involve individual occupants boarding and alighting the vehicle for different seating positions, including the driver seat, front passenger seat and the rear seats located behind the driver and front passenger. LC5 and LC6 simulate scenarios where two persons board and alight the vehicle simultaneously, either both in the front row or both in the back row. LC7 and LC8 address loading conditions, with 40 kg and 250 kg weights being placed in the trunk to simulate cargo. The individuals participating in the experiments weigh between 75 kg and 80 kg. The opening and closing of the doors or the trunk lid are taken into account in all LCs.

Table 1: Overview of LCs.

No.	LC	Position
1	boarding/alighting	driver seat
2	boarding/alighting	front passenger seat
3	boarding/alighting	behind driver seat
4	boarding/alighting	behind front passenger seat
5	boarding/alighting (2 passengers)	front row
6	boarding/alighting (2 passengers)	back row
7	loading/unloading (40 kg)	trunk
8	loading/unloading (250 kg)	trunk

A fiducial marker (AprilTag tag36h11) is used to track the motion of the vehicle inlet [6]. A six degrees-of-freedom (6-DOF) pose estimation is performed using the official AprilTag library [7], combined with a camera calibration provided by the OpenCV framework [8].

Video data is recorded using a GoPro HERO 9 camera at 200 frames per second with a resolution of 1920×1080 pixels in wide-angle mode. The camera is mounted on a tripod and positioned in front of the inlet (see Figure 1). The video recording captures the motion of an AprilTag marker attached to the inlet. For each frame of the video, the pose of the AprilTag is extracted and assigned a timestamp. The initial position is defined as a reference, and all subsequent movements are calculated relative to it, allowing the measurement to be independent of the camera's exact position. After processing the video material, a low-pass filter with a cutoff frequency of 2 Hz is applied to the recorded displacement and rotations. The movement velocity is determined by differentiating the relative displacement.

The coordinate system is defined relative to the camera. The x-axis points to the right, parallel to the ground plane and aligned with the vehicle's longitudinal axis. The y-axis extends forward through the camera lens, also parallel to the ground. The z-axis points upward, perpendicular to the ground. This coordinate system is chosen because it reflects

the physical mounting position of the camera in an aEVCS, for which the requirements are being developed.

Figure 1: Experimental setup showing the positioning of the camera system and AprilTag marker on a Ford Explorer.

The field of view (FOV) of the Camera is 118° horizontally and 69° vertically [9]. The width of the FOV can be calculated using the following formula [10]:

$$\text{width} = 2 \cdot d \cdot \tan\left(\frac{\theta}{2}\right)$$

In this equation, d denotes the distance from the camera to the object, and θ represents the full field-of-view angle. These parameters determine the physical width of the scene captured by the camera. AprilTag achieves sub-pixel-level localization accuracy with regard to the corners of the tag, particularly when the tag is fully visible and undistorted [6]. At a distance of 25 cm between the lens and the virtual pane, each pixel represents 0.317 mm in the vertical direction and 0.433 mm in the horizontal direction.

Table 2: Overview of vehicles.

Vehicle	Inlet position
Ford Explorer	rear-right
Ford Mustang Mach-E	front-left
Škoda Citigo-e iV	rear-right

The vehicles used in this study are listed in Table 2, along with the respective positions of their charging inlets, all of which are located on the fender.

3 Results and Discussion

Figure 2 presents representative measurements for LC1 and LC6, which involve one or two passenger boarding or alighting the vehicle, respectively. The test vehicle is a Ford

Explorer, with its charging inlet located on the rear-right side. As expected, the largest displacement occurred downward along the z-axis. When the front-row passenger boarded the vehicle (LC1), the inlet moved downward by 2.3 mm. For the two rear-row passengers (LC6), the displacement increased to 12.9 mm. The maximum velocity during boarding ranged from 7.7 mm/s for LC1 to 24.9 mm/s for LC6. Upon alighting, the inlet moved upward slightly more slowly, with velocities of 4.8 mm/s and 14.8 mm/s for LC1 and LC6, respectively. During boarding, the inlet also shifted slightly to the right along the x-axis, 2.6 mm for LC1 and LC6, indicating a minor forward translation of the vehicle. The peak velocity of this lateral motion was approximately 10 mm/s. The lateral displacement of the inlet along the y-axis resulting from LC1 ranged between 0 mm and 3.2 mm, whereas for LC6 it varied between -1.2 mm and 2.6 mm. Corresponding velocities ranged from -10.1 mm/s to 12.2 mm/s, and from -8.4 mm/s to 17.4 mm/s, respectively. Compared to linear displacements, rotational movements of the inlet were minimal under these conditions, with angular variations ranging between -0.6° and 0.6° across all axes.

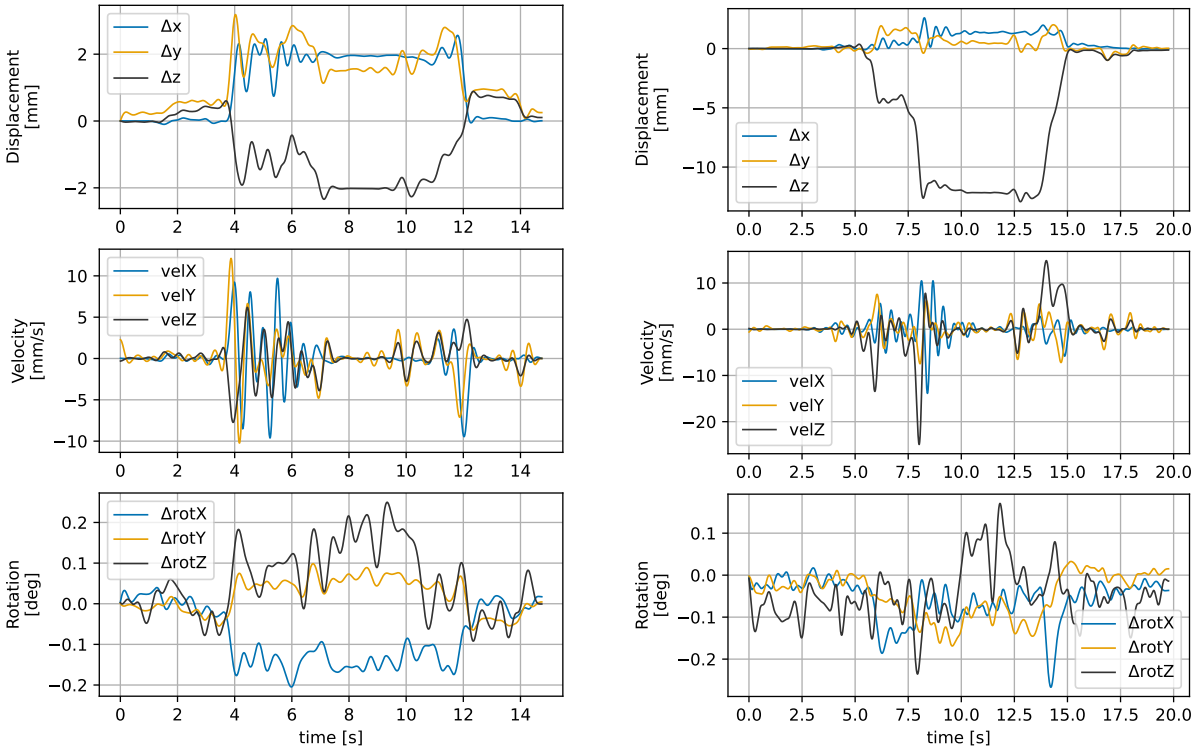

(a) (b)

Figure 2: Inlet displacement and velocity for LC1 (a) and LC6 (b) for Ford Explorer.

The limits for permissible inlet displacement and rotations during the docking, undocking, and charging operations between an EV and an aEVCS are specified in ISO 5474-5. In this standard, the coordinate system is specified according to ISO 4130. The origin is located at the center of the vehicle, the x-axis pointing toward the rear of the car, and the z-axis directed upward. The reference point for rotational movements is defined at the tip of the PE pin of the inlet [5]. The directions of the measured displacements along the x-, y-, and z-axes are aligned with the corresponding axes defined in ISO 4130. According to ISO 5474-5, the maximum permissible inlet displacements are ±70 mm along the z-axis, ±20 mm along the x-axis, and ±7 mm along the y-axis [5]. The allowable rotational limits are ±2° around the x- and y-axes, and ±1° around the z-axis [5].

Table 3 summarizes the minimum and maximum inlet displacements and rotations observed across selected LCs for all vehicles. Translational displacements are described by the x-, y-, and z-components, while rotational deflections are represented by rotX, rotY, and rotZ. Some values exceed the permissible limits specified in ISO 5474-5 and are highlighted in the table.

Table 3: Inlet motion limits for selected LCs across three test vehicles.

Parameter	Ford Explorer			Ford Mach-E			Škoda Citigo-e iV			
	LC1	LC5	LC6	LC1	LC5	LC6	LC1	LC5	LC6	LC8
$x_{\min}$ [mm]	-0.1	-0.1	-0.1	-2.5	-5.1	-2.4	-0.1	0.0	-0.4	-0.7
$x_{\max}$ [mm]	2.6	4.5	2.6	0.2	0.2	0.5	4.3	13.5	8.2	3.9
$y_{\min}$ [mm]	0.0	-1.2	-1.0	-2.5	-2.0	-2.5	-1.7	-1.6	-1.4	-1.4
$y_{\max}$ [mm]	3.2	2.6	2.0	1.5	2.5	1.2	5.8	6.3	6.4	3.2
$z_{\min}$ [mm]	-2.3	-7.3	-12.9	-6.5	-11.3	-6.4	-6.7	-20.1	-36.4	-50.3
$z_{\max}$ [mm]	0.9	0.3	0.4	0.4	1.4	0.3	1.3	0.8	0.2	1.0
$rotX_{\min}$ [°]	-0.4	-0.3	-0.4	-0.5	-0.8	-0.5	-0.5	-1.3	-2.1	-2.9
$rotX_{\max}$ [°]	0.1	0.2	0.2	0.4	0.5	0.4	0.5	3.5	2.5	2.4
$rotY_{\min}$ [°]	-0.1	-0.1	-0.3	-0.1	-0.2	-0.1	-0.1	-0.2	-1.2	-2.1
$rotY_{\max}$ [°]	0.2	0.2	0.2	0.1	0.1	0.3	0.1	0.1	0.0	0.0
$rotZ_{\min}$ [°]	-0.4	-0.5	-0.6	-0.9	-1.5	-1.0	-0.4	-2.2	-0.2	-0.1
$rotZ_{\max}$ [°]	0.6	0.3	0.4	0.7	1.0	0.4	0.2	0.7	1.6	2.3

The largest displacement along the z-axis was observed for the Škoda Citigo-e iV under LC8, with a value of -50.3 mm. In this case, 250 kg were loaded into the trunk of the compact vehicle, corresponding to approximately 85% of its maximum payload capacity [11]. Despite this comparatively high loading condition, the resulting inlet displacement was 72% of the allowable maximum. For the other vehicles, the maximum measured displacement along the z-axis was -12.9 mm, which remains well within the permissible range. Along the x-axis, the maximum displacement was 13.5 mm and the only value exceeding 10 mm. The limit in ISO 5474-5 is substantially higher than all observed values, indicating a considerable margin relative to the displacements recorded in the tests. The smallest inlet displacements were recorded along the y-axis, with a maximum value of 6.4 mm. The measured values remain within the defined limit, indicating that the threshold adequately covers the displacements observed under the given test conditions.

The maximum rotational values measured for the Škoda Citigo-e iV show that these limits are exceeded for all three axes. For the rotation around the x-axis, three measurements fell outside the permissible range, with a maximum of 3.5° observed in LC5 for the Citigo. Regarding rotation around the y-axis, the minimum value of -2.1° in LC8 slightly exceeds the allowable limit, while the extreme values of all other measurements remain well within the ±2° boundary. Furthermore, the limits for rotation around the z-axis of ±1° were exceeded in measurements of the Citigo in LC5, LC6, and LC8, with a maximum value of 2.3°, which is clearly outside the permissible range. Also, the rotation limit around the z-axis was exceeded in the Ford Mustang Mach-E measurement during LC5. This analysis reveals that multiple vehicles and loading scenarios result in inlet movements exceeding ISO 5474-5 thresholds, suggesting a need to refine these standards to better reflect real-world variability.

A comparison of the maximum inlet displacement along the z-axis in LC1, in which a passenger boards and alights the driver's seat, shows that vehicle size, weight, and inlet position significantly influence inlet movement. The smallest displacement of -2.3 mm was observed for the Ford Explorer. Under the same loading condition, the Ford Mustang Mach-E exhibited a larger displacement of -6.5 mm, which is consistent with the inlet's front-left position near the driver's seat. The Škoda Citigo-e iV showed a displacement of -6.7 mm, similar to the Mach-E, despite having an inlet position comparable to that of the Explorer. However, the Citigo's smaller dimensions and significantly lower weight (1235 kg) [11] suggest a more compliant suspension setup, which may explain the greater vertical inlet displacement observed in comparison to the heavier vehicles. The Explorer (1908 kg) [12] and the Mach-E (2044 kg) [13] are relatively similar in overall weight, especially when contrasted with the much lighter Citigo. These findings reinforce that inlet displacement for a given LCis influenced by both the inlet position and the vehicle characteristics.

According to [14], the permitted misalignment for docking is ±3 mm along the x-axis and ±5 mm along the y-axis. To investigate the geometric tolerances of automated docking, this study employs an industrial robot equipped with a CCS Combo 2 connector, engaging with an inlet mounted on a spring-supported cardanic suspension. All measurements for LC5, as well as all LCs for the Citigo, exceed the permissible threshold along the x-axis. For the y-axis, the Citigo exceeds the threshold in LC1, LC5, and LC6. These results suggest that certain vehicle movements during the docking procedure may lead to failed connection attempts. Therefore, external influences during docking should be minimized, as the allowable tolerances, especially along the x-axis, are significantly tighter than those during the charging process.

4 Conclusion

This study offers preliminary insights into the movement of electric vehicle inlets under real-world conditions and establishes a foundation for developing practical requirements for aEVCS. Initial measurements suggest that the translational movement of inlets typically remains within normative limits with additional safety margins. However, rotational movements frequently approach or exceed threshold values, particularly in smaller vehicles. This suggests that current standards may not fully reflect real-world variability. As in ISO 5474-5, the analysis considers only real-world scenarios, explicitly excluding extreme load cases, such as those involving vandalism.

Preliminary reference values for inlet movement speed have been established, though more measurements are needed for statistically valid generalizations. Furthermore, the inlet's position (front or rear) may significantly influence movement characteristics, underscoring the need to study a broader range of vehicle types.

Several load cases, particularly those involving the Citigo, exceeded the functional limits of the connector/inlet capture capability. This indicates that specific vehicle dynamics may result in docking failures, highlighting the importance of minimizing external influences during docking.

Overall, this study provides an initial overview that highlights the need for further research. A more diverse vehicle selection, especially of small vans, as well as an expanded dataset,

are essential for defining robust, evidence-based threshold values and ensuring reliable, standardized performance across a wide range of conditions.

Acknowledgment

This research was supported by the Federal Republic of Germany through funding from the Federal Ministry for Economic Affairs and Energy (BMWE) due to a decision of the German Bundestag under grant number 01MV22008A (RuBakaL).

The authors gratefully acknowledge Ford-Werke GmbH for supplying vehicles used in the experimental testing.

References

[1] Panagiotis Skaloumpakas et al. "A user-friendly electric vehicle reallocation solution for uniformly utilized charging stations". en. In: *Sustainable Energy, Grids and Networks* 38 (June 2024), p. 101266. DOI: 10.1016/j.segan.2023.101266.

[2] Oussama Alyounes, Miguel Altamirano Cabrera, Dzmitry Tsetserukou. *HaptiCharger: Robotic Charging of Electric Vehicles Based on Human Haptic Patterns*. 2023. DOI: 10.48550/ARXIV.2310.09346.

[3] Bahar Azin, Xianfeng (Terry) Yang, Nikola Marković, Mingxi Liu. "Infrastructure enabled and electrified automation: Charging facility planning for cleaner smart mobility". en. In: *Transportation Research Part D: Transport and Environment* 101 (Dec. 2021), p. 103079. DOI: 10.1016/j.trd.2021.103079.

[4] Jens Bucher, Jan Knipschild, Bernd Künne. "Development and evaluation of an automatic connection device for electric cars with four DOFs and a control scheme based on infrared markers". en. In: *International Journal of Mechatronics and Automation* 8.4 (2021), p. 175. DOI: 10.1504/IJMA.2021.120378.

[5] International Organization for Standardization. *ISO 5474-5: Road vehicles - Electrical connectors - Part 5: Test methods and general performance requirements*. Standard. 2022.

[6] Edwin Olson. "AprilTag: A robust and flexible visual fiducial system". In: *2011 IEEE International Conference on Robotics and Automation*. May 2011, pp. 3400–3407. DOI: 10.1109/ICRA.2011.5979561.

[7] *AprilRobotics/apriltag*. May 2025. URL: https://github.com/AprilRobotics/apriltag (visited on 05/22/2025).

[8] *OpenCV: Camera Calibration*. URL: https://docs.opencv.org/4.x/dc/dbb/tutorial_py_calibration.html (visited on 05/22/2025).

[9] *GoPro Support*. URL: https://community.gopro.com/s/article/HERO9-Black-Digital-Lenses-FOV-Information (visited on 05/30/2025).

[10] Richard Szeliski. *Computer Vision: Algorithms and Applications*. en. Texts in Computer Science. London: Springer London, 2011. DOI: 10.1007/978-1-84882-935-0.

[11] EV Database. *Skoda CITIGO e iV*. URL: https://ev-database.org/de/pkw/1190/Skoda-CITIGO-e-iV (visited on 05/30/2025).

[12] EV Database. *Ford Explorer Standard Range RWD*. URL: https://ev-database.org/de/pkw/2167/Ford-Explorer-Standard-Range-RWD (visited on 05/30/2025).

[13] EV Database. *Ford Mustang Mach-E Standard Range (MY23.75)*. URL: https://ev-database.org/de/pkw/1242/Ford-Mustang-Mach-E-Standard-Range (visited on 05/30/2025).

[14] T. Bergmann. "Fangraumanalyse zur Beurteilung eines Stecksystems". Unpublished Seminar paper. Dortmund, Germany, 2015.